Pergamon

Int. J. Solids Structures Vol. 33, No. 2, pp. 283–299, 1996

0020–7683/96 $9.50 + .00

0020–7683(95)00029–1

DEFORMATION OF SIMPLY SUPPORTED CIRCULAR PLATE BY CENTRAL PRESSURE PULSE

DONGQUAN LIU and W. J. STRONGE
Department of Engineering, University of Cambridge, Trumpington Street, Cambridge CB2 1PZ, U.K.

(*Received* 20 *July* 1994; *in revised form* 20 *January* 1995)

Abstract—Bending of a circular simply supported plate subjected to a central pressure pulse is investigated theoretically: the plate is assumed to be rigid perfectly-plastic and follows the Tresca yield condition. Results are presented for a central pulse of constant pressure and brief duration. If the blast pressure is sufficiently large the radial bending moment changes sign between the region of loading and the periphery of the plate. Previous analyses of pulse loading on a simply supported rigid–plastic plate gave bending moments that satisfied the yield condition only if the pressure magnitude was not very large. The present analysis extends the previous analyses into the range of large pressures.

1. INTRODUCTION

For ductile materials, the rigid–plastic idealization considerably simplifies theoretical investigations into the response of dynamically loaded structures which undergo moderately large plastic deformations. The rigid–plastic idealization can provide estimates of dynamic response for a wide range of practical problems if the energy dissipated by elastic deformation is much less than the energy dissipated by plastic deformation and if the pulse duration is brief (Stronge and Yu, 1993). Past work on the dynamic deformation of a rigid–plastic simply supported circular plate concerned blast loading where the pressure varies with both radial position and time. Hopkins and Prager (1954) found the response of a simply supported plate to a rectangular pulse distributed uniformly over the entire area. Using a similar method of solution, Conroy (1969) investigated the deformation produced by a central pulse of constant amplitude. Youngdahl (1971, 1987) obtained plate deformation for other pulse shapes and arbitrary axisymmetric pressure distributions.

A general feature of these rigid–plastic solutions is a transient phase with velocity patterns involving travelling hinges or hinge bands, followed by a modal phase of deformation. In the above solutions for a simply supported circular plate, the velocity pattern in the transient phase includes a central part with uniform transverse velocity $\dot{W}_0(T)$ surrounded by an annular region with a velocity distribution that varies linearly with radius r [Fig. 1(c)]. The boundary between the two areas is a hinge circle $r = r_0$ which travels towards the plate centre; in the modal response phase the velocity pattern is conical for the entire plate [Fig. 1(a)]. Corresponding to the above velocity field, stresses in the plate are assumed to be on face AB of the Tresca yield surface (Fig. 2) where the circumferential bending moment M_θ is equal to the fully plastic bending moment M_0 while the radial bending moment M_r varies between zero and M_0. If the above velocity pattern is used for the case of a central pressure pulse the radial bending moment M_r can change sign in a simply supported plate. This case occurs if the blast pressure is so large that at the periphery of the plate $r = R$ the gradient of the radial moment $\partial M_r/\partial r > 0$. This limitation was noticed by Conroy (1969), but she did not analyse this case. For a simply supported beam under partly distributed blast loading a similar problem was discussed by Jones and Song (1986).

The present theoretical study focuses attention on the dynamic response of a simply supported rigid-plastic plate subjected to blast loading over a central area; the loading is large enough to cause a change of sign of the radial bending moment in the plate near the periphery. Six different patterns of motion are obtained (Fig. 1). The ranges of the parameters are related to the load magnitude and size of the loaded area for a variety of patterns of initial motion. Results are presented for a pressure P_0 applied in a central region

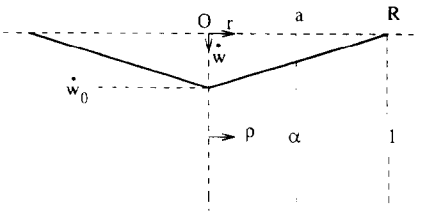

(a) Mechanism 1

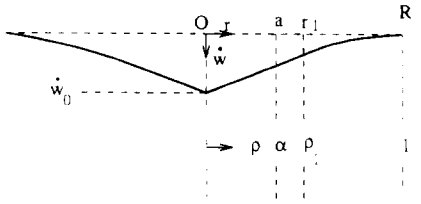

(b) Mechanism 2a

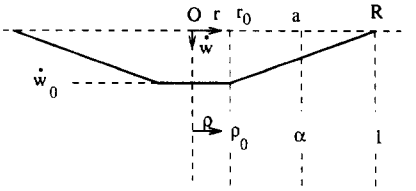

(c) Mechanism 2b

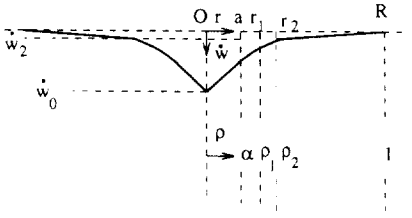

(d) Mechanism 3a

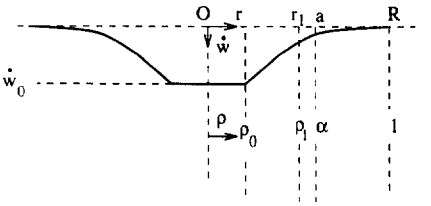

(e) Mechanism 3b

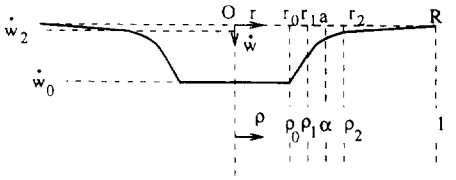

(f) Mechanism 4

Fig. 1. Velocity patterns of a simply supported plate.

of radius a; the pressure is suddenly applied at time $T = 0$ and then later removed after a period T_0. The final central deflection of a simply supported plate predicted by this analysis and the previous analyses, which are satisfactory only for the pressure acting on the entire plate, are compared to clarify the effect of different assumptions for yield. The influence of the support condition at the plate periphery (simply supported or clamped) on the final central deflection is investigated by comparing Florence's solution for a clamped plate (Florence, 1966a, b) with the present solution for a simply supported plate.

2. GENERAL DETAILS

2.1. *Equations of motion for a circular plate*

For small axisymmetric deformation of a circular plate, the equations of motion are

$$\frac{\partial(rM_r)}{\partial r} - M_\theta = rQ_r \tag{1}$$

and

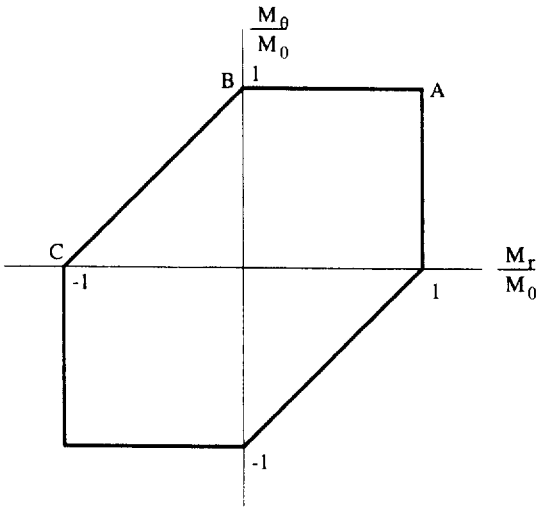

Fig. 2. The Tresca yield condition.

$$\frac{1}{r}\frac{\partial(rQ_r)}{\partial r} = -p(T) + \mu\frac{\partial^2 W}{\partial T^2}, \tag{2}$$

where M_r, M_θ are the radial and circumferential bending moments per unit length, Q_r is the shear force per unit length, T is time, $p(T)$ is pressure per unit area of the plate, W is plate transverse displacement and μ is the mass density per unit area of the plate. Rotatory inertia is neglected.

If radial displacements are negligible the curvature rates are given by

$$\dot{K}_r = -\frac{\partial^2 \dot{W}}{\partial r^2}, \quad \dot{K}_\theta = -\frac{1}{r}\frac{\partial \dot{W}}{\partial r}. \tag{3}$$

For a rigid–plastic plate the fully plastic bending moment $M_0 = \sigma_y H^2/4$ and transverse shear force $Q_0 = \sigma_y H/2$ are structural parameters, where σ_y is the flow stress of the plate material and H is the plate thickness. In the present study shear deformation is assumed to be negligible.

Non-dimensional variables in these equations are used in the following. They are defined as: $m_r = M_r/M_0$, $m_\theta = M_\theta/M_0$, $q_r = Q_r/Q_0$, $\rho = r/R$, $w = W/H$, $k_r = K_r R^2/H$, $k_\theta = K_\theta R^2/H$, $v = R/H$ and $t = T\sqrt{(2Q_0/\mu)}/H$. In the following, $m_r(\rho)$ describes the radial bending moment as a function of ρ.

2.2. *Yield condition and flow rule*

We consider a plate made of rigid plastic material which obeys the Tresca yield condition shown in Fig. 2 and an associated flow rule. The present study will involve only yield states on the part ABC of the yield surface so only the following regimes need be considered:

$$\begin{aligned}
&\text{Regime A:} \quad m_r = m_\theta = 1 : \dot{k}_r : \dot{k}_\theta = (1-\lambda) : \lambda ;\\
&\text{Regime AB:} \quad 0 < m_r < 1, m_\theta = 1 : \dot{k}_r : \dot{k}_\theta = 0 : 1 ;\\
&\text{Regime B:} \quad m_r = 0, m_\theta = 1 : \dot{k}_r : \dot{k}_\theta = -\lambda : 1 ;\\
&\text{Regime BC:} \quad -1 < m_r < 0, m_\theta = 1 + m_r : \dot{k}_r : \dot{k}_\theta = -1 : 1 ;\\
&\text{Regime C:} \quad m_r = -1, m_\theta = 0 : \dot{k}_r : \dot{k}_\theta = -1 : (1-\lambda) ;
\end{aligned} \tag{4}$$

the constant λ is in the range $0 \leqslant \lambda \leqslant 1$.

There is a possibility that part of the plate is not yielding at a given instant. In such a case at this instant this part moves as a rigid body. In view of rotational symmetry and the lack of radial displacement, such a part can have, at most, a uniform vertical velocity.

2.3. *Method of solution*

The technique used to obtain bending moments and deflection is first to obtain a velocity field of the plate and then to integrate the equations of motion. The velocity field for a complete solution must satisfy:

(1) equations of motion (1) and (2);
(2) initial conditions $W(r, 0) = \dot{W}(r, 0) = 0$ or $w(\rho, 0) = \dot{w}(\rho, 0) = 0$;
(3) the Tresca yield condition and an associated flow rule;
(4) the necessary continuity and discontinuity conditions in space and time.

The continuity and discontinuity conditions were discussed in detail by Hopkins and Prager (1954). For the present problem the following conclusions can be reached:

(1) across a hinge circle (travelling or stationary) the transverse shear force and radial bending moment are continuous;
(2) since the rotatory inertia is neglected, discontinuities in curvature, angular velocity and transverse acceleration are possible across a travelling hinge circle.

3. MECHANISMS OF DEFORMATION AND GOVERNING EQUATIONS

A blast pulse is usually described as an exponentially decreasing function of time; it has an instantaneous rise to the peak pressure p_0 followed by a continuous monotonic decay. At instant t after blast the pressure can be expressed as $p = p_0 f(t)$, where $f(t)$ is a continuous monotonic decay function with $f(0) = 1$. This form of pulse results in a deformation field that progresses steadily through a sequence of mechanisms.

The static limit loading p_s acting on a central circular area of radius a can be expressed in non-dimensional form as (Hopkins and Prager, 1953):

$$\mu_s \equiv p_s R^2/2M_0 = \frac{3}{\alpha^2(3-2\alpha)}, \tag{5}$$

where the relative size of the loaded area $\alpha = a/R$.

During deformation the plate is divided into annular regions where each has a stress state on a vertex or side of the Tresca yield condition (Fig. 2). The simple velocity patterns used by previous authors [Figs 1(a, c)] were compatible with only the portion AB of the Tresca yield condition. For a pulse of intermediate pressure, e.g. $p_0/p_s = 2$ as shown in Fig. 3, these produce a negative radial bending moment when the radial change in moment at the edge of the plate $\partial m_r/\partial\rho|_{\rho=1} > 0$; for a pulse of large pressure, e.g. $p_0/p_s = 10$ as shown in Fig. 3, the radial bending moment is negative and large enough to exceed the negative fully plastic bending moment M_0. To obtain a solution which satisfies yield throughout the plate, the present study employs a more complex velocity field corresponding to stresses on portions ABC of the yield surface. This velocity field has distinct annular regions wherein the flow rule, boundary conditions and the appropriate continuity and discontinuity conditions are satisfied (see the above section).

For a blast pulse with a large value of peak pressure $\mu_0 \equiv p_0 R^2/2M_0$ in excess of the static limit loading μ_s, the plate commences motion in one of six mechanisms (Fig. 1) depending on the pressure μ_0/μ_s and the radius of loaded region $\alpha \equiv a/R$ (Fig. 4).

3.1. *Motion beginning with mechanism* 1

For small values of μ_0, it is assumed that motion commences in the static collapse mechanism 1 with a conical velocity distribution that was described in the Section 1 [Fig.

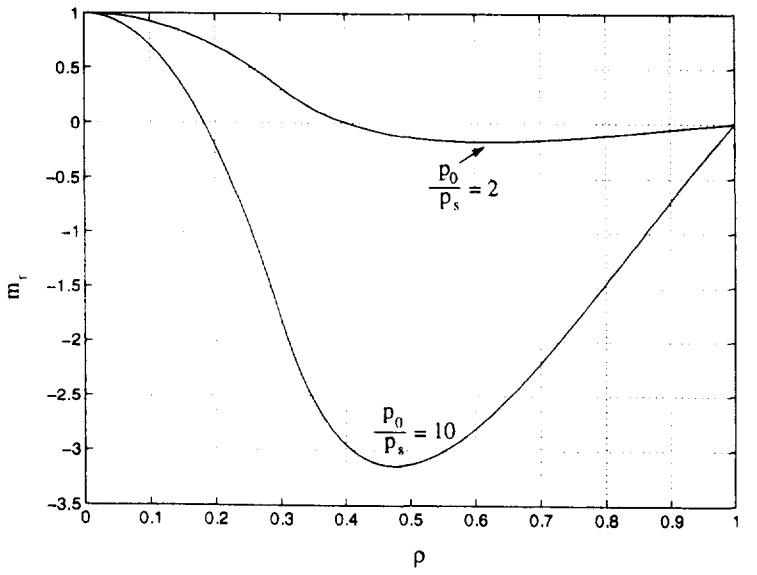

Fig. 3. Radial bending moment in plate resulting from the conical velocity pattern M 1 for loaded region $\alpha = 0.3$ and pressures $p_0/p_s = 2$ and 10.

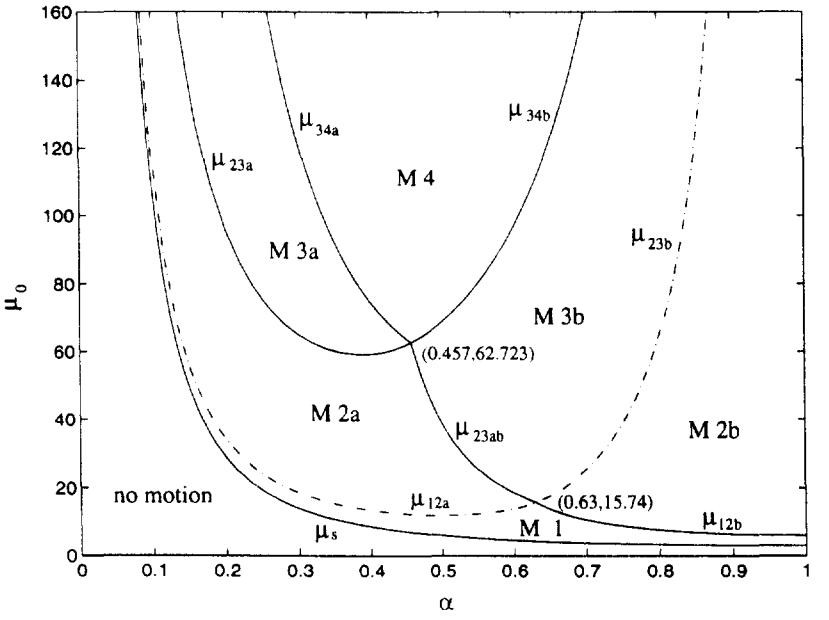

Fig. 4. Mechanisms of initial motion.

1(a)]. This velocity pattern is expressed as

$$\dot{w}(\rho, t) = \dot{w}_0(t)(1-\rho) \quad (0 \leqslant \rho \leqslant 1), \tag{6}$$

where $\dot{w}_0$ is the velocity at the centre of the plate. With this velocity field and the bending moment state described in Section 1, the equations of motion furnish the result (Conroy, 1969):

$$m_r = \begin{cases} 1 - \{\mu_0 f(t)\rho^2 - (2\rho^2 - \rho^3)[\mu_0 f(t)\alpha^2(3-2\alpha) - 3]\}/3 & 0 \leqslant \rho \leqslant \alpha \\ 1 - \mu_0 f(t)\alpha^2 + [2\mu_0 f(t)\alpha^3/3\rho] + (2\rho^2 - \rho^3)[\mu_0 f(t)\alpha^2(3-2\alpha) - 3]/3 & \alpha \leqslant \rho \leqslant 1 \end{cases} \tag{7}$$

and

$$\ddot{w}_0(t) = \mu_0 f(t)\alpha^2(3-2\alpha) - 3. \tag{8}$$

Analysis of eqn (7) shows that the deformation of a plate begins in mechanism 1 (Fig. 4) if

$$\mu_s < \mu_0 \leqslant \mu_{12a} \equiv \frac{3}{\alpha^2(3-4\alpha)} \qquad (0 < \alpha < 0.63)$$

$$\mu_s < \mu_0 \leqslant \mu_{12b} \equiv \frac{6}{6\alpha^2 - 4\alpha^3 - 1} \quad (0.63 \leqslant \alpha \leqslant 1), \tag{9}$$

where μ_{12a} and μ_{12b} are limiting pressures of mechanism 1; at larger pressures the plate deforms in either mechanism 2a or 2b in order to satisfy the yield condition. For a loading radius $\alpha = 0.63$ and a pressure $\mu_0 = 15.74$, the radial bending moment m_r is maximum at the centre ($\partial^2 m_r/\partial\rho^2|_{\rho=0} = 0$) while simultaneously it is a minimum at the periphery ($\partial m_r/\partial\rho|_{\rho=1} = 0$). For a small loaded region $0 < \alpha < 0.63$, if the pressure $\mu_0 = \mu_{12a}$, the radial moment m_r is just a minimum at the periphery ($\partial m_r/\partial\rho|_{\rho=1} = 0$) while m_r is always a maximum at the centre ($\partial^2 m_r/\partial\rho^2|_{\rho=0} \leqslant 0$); for a large loaded region $0.63 < \alpha \leqslant 1$, if the pressure $\mu_0 = \mu_{12b}$, the radial moment m_r is just a maximum at the centre ($\partial^2 m_r/\partial\rho^2|_{\rho=0} = 0$) while m_r is always a minimum at the periphery ($\partial m_r/\partial\rho|_{\rho=1} < 0$).

3.2. *Motion beginning in mechanism 2a*

For $0 < \alpha \leqslant 0.63$, if the peak pressure μ_0 is greater than μ_{12a}, the radial moment m_r obtained from the velocity pattern (6) of mechanism 1 violates the condition $m_r \geqslant 0$ in the neighbourhood of the plate periphery, $\rho = 1$. This suggests a different mechanism of deformation known as 2a where bending moments m_r and m_θ are assumed to obey the following conditions:

(1) In an inner portion $0 \leqslant \rho \leqslant \rho_1$, bending moments are in regime AB of the Tresca yield condition where the radial bending moment $m_r(\rho)$ decreases monotonically from its value $m_r(0) = 1$ to $m_r(\rho_1) = 0$.

(2) In the outer portion $\rho_1 \leqslant \rho \leqslant 1$, bending moments are in regime BC of the Tresca yield condition where the radial bending moment $m_r(\rho)$ decreases from its value $m_r(\rho_1) = 0$ to a minimum somewhere between $\rho = \rho_1$ and $\rho = 1$ and afterwards increases to vanish at the simply supported edge $\rho = 1$. The minimum value of m_r is larger than -1.

It can be seen that the circle at $\rho = \rho_1$ divides the plate into two regions. Across this circle, there exists a discontinuity in radial curvature rate; however, the radial rate of rotation across this boundary must be continuous since the radial bending moment at the circle is not fully plastic. Employing the flow rules for deformation, the velocity field can be obtained by noticing the velocity boundary condition. This produces the velocity pattern of the mechanism 2a [Fig. 1(b)]:

$$\dot{w} = \begin{cases} \dot{w}_0[1 - \sigma\rho/\rho_1] & 0 \leqslant \rho \leqslant \rho_1(t) \\ \dot{w}_0\sigma\ln(1/\rho) & \rho_1(t) \leqslant \rho \leqslant 1 \end{cases} \tag{10}$$

where $\sigma = [\ln(1/\rho_1) + 1]^{-1}$. It is evident that this velocity pattern includes a central part with a linear velocity distribution associated with section AB of the yield surface. This is surrounded by an annular region with a velocity distribution that varies logarithmically with radius ρ which is associated with section BC of the yield surface [Fig. 1(b)].

The acceleration to be substituted in eqn (2) can be obtained by differentiating the velocity field (10). rQ_r is obtained by integration of eqn (2) and then substituted into eqn (1). With the use of the yield condition (Fig. 2) the circumferential bending moment is eliminated from eqn (1). Integrating eqn (1) in annular regions $0 \leqslant \rho \leqslant \rho_1(t)$ and

$\rho_1(t) \leqslant \rho \leqslant 1$, respectively, with the interface conditions $m_r(\rho_1) = 0$ and $m_r(1) = 0$, yields the following equations

$$v^2\ddot{w}_0(2\xi_1+1)(\xi_1+1) - v^2\dot{w}_0\dot{\xi}_1\xi_1 = \begin{cases} \{\mu_0 f(t)(3\alpha^2 e^{2\xi_1} - 2\alpha^3 e^{3\xi_1}) - 3e^{2\xi_1}\}(\xi_1+1)^2 & (\rho_1 > \alpha) \\ \{\mu_0 f(t) - 3e^{2\xi_1}\}(\xi_1+1)^2 & (\rho_1 \leqslant \alpha) \end{cases} \tag{11}$$

$$v^2\ddot{w}_0\{3e^{2\xi_1} - 3 - 4\xi_1\}(\xi_1+1) + v^2\dot{w}_0\dot{\xi}_1\{-3e^{2\xi_1} + 3 + 6\xi_1 + 2\xi_1^2\} = \begin{cases} 3\{\mu_0 f(t)\alpha^2 - 1\}\xi_1(\xi_1+1)^2 e^{2\xi_1} & (\rho_1 > \alpha) \\ 3\left\{\frac{1}{2}\mu_0 f(t)\alpha^2\left(1 + 2\ln\frac{1}{\alpha} - \frac{e^{2\xi_1}}{\alpha^2}\right) - \xi_1\right\}(\xi_1+1)^2 e^{2\xi_1} & (\rho_1 \leqslant \alpha) \end{cases} \tag{12}$$

where $\xi_1 = \ln(1/\rho_1)$. With the use of the initial condition $\dot{w}_0 = 0$ at $t = 0$, the above equations reduce to

$$v^2\ddot{w}_0(2\xi_1+1) = \begin{cases} \{\mu_0[3\alpha^2 e^{2\xi_1} - 2\alpha^3 e^{3\xi_1}] - 3e^{2\xi_1}\}(\xi_1+1) & (\rho_1 > \alpha) \\ \{\mu_0 - 3e^{2\xi_1}\}(\xi_1+1) & (\rho_1 \leqslant \alpha) \end{cases} \tag{13}$$

$$v^2\ddot{w}_0\{3e^{2\xi_1} - 3 - 4\xi_1\} = \begin{cases} 3[\mu_0\alpha^2 - 1]\xi_1(\xi_1+1)e^{2\xi_1} & (\rho_1 > \alpha) \\ 3\left\{\frac{1}{2}\mu_0\alpha^2\left(1 + 2\ln\frac{1}{\alpha} - \frac{e^{2\xi_1}}{\alpha^2}\right) - \xi_1\right\}(\xi_1+1)e^{2\xi_1} & (\rho_1 \leqslant \alpha) \end{cases} \tag{14}$$

These expressions provide the initial values of $\xi_1(\alpha, \mu_0)$ and $\ddot{w}_0(\alpha, \mu_0)$. In the mechanisms described in the following, initial values of variables representing hinge positions are obtained in the same way as those in mechanism 2a so that the method will not be repeated again.

In order that radial bending moment m_r is a maximum at the centre and that the minimum value of m_r at $\rho = \rho_2$ in the annulus $\rho_1 \leqslant \rho \leqslant 1$ does not exceed the negative fully plastic bending moment at time $t = 0$, we must ensure that $\partial^2 m_r/\partial\rho^2|_{\rho=0} \leqslant 0$ while $\partial m_r/\partial\rho|_{\rho=\rho_2} = 0$ and $m_r(\rho_2) \geqslant -1$ are satisfied simultaneously. For an intermediate radius of loading $0.457 < \alpha < 0.63$, it is found that with more intense pressure a maximum radial bending moment is first reached at the centre where $\partial^2 m_r/\partial\rho^2|_{\rho=0} = 0$. This is represented by

$$2v^2\ddot{w}_0 = \mu_0. \tag{15}$$

For a small radius of loading $0 < \alpha < 0.457$, the minimum value of m_r in annulus $\rho_1 \leqslant \rho \leqslant 1$ reaches the negative fully plastic bending moment first where $\partial m_r/\partial\rho|_{\rho=\rho_2} = 0$ and $m_r(\rho_2) = -1$. The above two conditions are represented by

$$v^2\ddot{w}_0\{3(2\xi_2+1)e^{2(\xi_1-\xi_2)} - 1\} = 3(\mu_0\alpha^2 - 1)(\xi_1+1)e^{2\xi_1} \tag{16}$$

$$v^2\ddot{w}_0\{e^{2\xi_2} - 1 - 2\xi_2 - 2\xi_2^2\} = (1+\xi_1)e^{2\xi_2}, \tag{17}$$

where $\xi_2 = \ln(1/\rho_2)$. Thus deformation of a plate begins in mechanism 2a if

$$\begin{aligned} &\mu_{12a} < \mu_0 \leqslant \mu_{23a} \qquad (0 < \alpha < 0.457) \\ &\mu_{12a} < \mu_0 \leqslant \mu_{23ab} \quad (0.457 < \alpha < 0.63). \end{aligned} \tag{18}$$

When $\mu_0 = \mu_{23a}$, eqns (16) and (17) are satisfied by the solutions $\dot{w}_0$ and ξ of eqns (13) and (14) while μ_{23ab} is determined by eqn (15). μ_{23a} and μ_{23ab} are limiting pressures for mechanism 2a which is bounded above by mechanisms 3a and 3b (Fig. 4). The equations for these limiting pressures are solved by an iteration subroutine for non-linear algebraic equations from the NAG Fortran library. Limiting pressures for other mechanisms described in the following are obtained in the same way as that for μ_{23a} or μ_{23ab} so the solution procedure will not be repeated.

3.3. *Motion beginning in mechanism 2b*

If the loaded area is large, $0.63 < \alpha \leqslant 1$ and the peak pressure μ_0 is greater than μ_{12b}, the yield condition for mechanism 1 is violated near the centre since the radial bending moment is not maximum at the centre. When $\partial^2 m_r(0)/\partial\rho^2 > 0$ a mechanism of deformation known as mechanism 2b is suggested where the velocity pattern is illustrated in Fig. 1(c). Previous authors have used this mechanism for the transient phase of deformation. The velocity field for mechanism 2b can be expressed as:

$$\dot{w}(\rho, t) = \begin{cases} \dot{w}_0(t) & (0 \leqslant \rho \leqslant \rho_0(t)) \\ \dot{w}_0(t)\dfrac{(1-\rho)}{(1-\rho_0)} & (\rho_0(t) \leqslant \rho \leqslant 1) \end{cases} \tag{19}$$

where the non-dimensional radius of the hinge circle $\rho_0 = r_0/R$. Equations which give the solution of $\dot{w}_0(t)$ and ρ_0 are

$$2v^2\ddot{w}_0 = \mu_0 f(t) \tag{20}$$

$$v^2\ddot{w}_0(1-\rho_0)(1+2\rho_0+3\rho_0^2) + v^2\dot{w}_0\dot{\rho}_0(1-\rho_0)(1+3\rho_0) = \mu_0 f(t)(3\alpha^2 - \rho_0^3 - 2\alpha^3) - 3. \tag{21}$$

Now, for $0.63 < \alpha \leqslant 1$, if

$$\mu_{12b} < \mu_0 \leqslant \mu_{23b} \tag{22}$$

the deformation of a plate begins to move in mechanism 2b (Fig. 4). For $\mu_0 \leqslant \mu_{23b}$, the radial bending moment is a minimum at the periphery $(\partial m_r/\partial\rho|_{\rho=1} = 0)$.

3.4. *Motion beginning in mechanism 3a*

In mechanism 2a, if the peak pressure μ_0 is greater than μ_{23a} for $0 < \alpha < 0.457$, the minimum value of the radial bending moment m_r exceeds the negative fully plastic bending moment in the portion $\rho_1 \geqslant \rho \geqslant 1$. The condition for motion beginning in mechanism 2a is violated. In this case it is assumed that motion begins in mechanism 3a where the plate is divided into three parts by the circle at $\rho = \rho_1$ and a hinge circle at $\rho = \rho_2$. Bending moments in the plate are assumed to obey the following conditions: (1) in the portion $0 \geqslant \rho \geqslant \rho_1$, the bending moments satisfy $0 \leqslant m_r \leqslant 1, m_\theta = 1$; (2) in the portions $\rho_1 \geqslant \rho \geqslant \rho_2$ and $\rho_2 \geqslant \rho \geqslant 1$, the bending moments are in the ranges $-1 \leqslant m_r \leqslant 0$, $m_\theta = 1 + m_r$. The radial bending moment m_r is a minimum at the circle of radius ρ_2, $m_r(\rho_2) = -1$. The velocity

field obtained from the flow rule that is compatible with the bending moments above will be [Fig. 1(d)]

$$\dot{w}(\rho,t)=\begin{cases}\dot{w}_2+(\dot{w}_0-\dot{w}_2)[1-\sigma_1\rho/\rho_1] & 0\leqslant\rho\leqslant\rho_1(t)\\ \dot{w}_2+(\dot{w}_0-\dot{w}_2)\sigma_1\ln\dfrac{\rho_2}{\rho} & \rho_1(t)\leqslant\rho\leqslant\rho_2(t)\\ \dot{w}_2\dfrac{\ln\rho}{\ln\rho_2} & \rho_2(t)\leqslant\rho\leqslant 1\end{cases}\tag{23}$$

where $1/\sigma_1=\ln(\rho_2/\rho_1)+1$ and $\dot{w}_2$ is the transverse velocity at the radius $\rho=\rho_2$. This velocity distribution produces a discontinuity of the radial rate of rotation across the circle of radius ρ_2 [Fig. 1(d)].

With $m_r(0)=1$, $m_r(\rho_1)=0$, $m_r(\rho_2)=-1$, $\partial m_r/\partial\rho|_{\rho=\rho_2}=0$ and $m_r(1)=0$ and transformations $\xi_1=\ln(1/\rho_1)$ and $\xi_2=\ln(1/\rho_2)$, integrating the equations of motion gives the governing equations; they are given later as eqns (32)–(35) with $\eta\equiv 1$.

At the outer hinge circle of radius ρ_2, the radial bending moment is a minimum. At ρ_2^-, $\partial m_r/\partial\rho\leqslant 0$ while at ρ_2^+, $\partial m_r/\partial\rho\geqslant 0$. Because $m_\theta-m_r=1$ in the neighbourhood of $\rho=\rho_2$ eqn (1) requires that the radial rate of change of the radial bending moment is continuous across this hinge circle, $\partial m_r/\partial\rho|_{\rho=\rho_2}=\partial m_r/\partial\rho|_{\rho=\rho_2^-}=0$. If this were not the case the transverse shear force would not be continuous across the hinge circle at $\rho=\rho_2$.

Now, for $0<\alpha<0.457$ and a large range of pressure

$$\mu_{23a}<\mu_0\leqslant\mu_{34a}\tag{24}$$

a plate begins to move in mechanism 3a (Fig. 4). If $\mu_0\leqslant\mu_{34a}$ the radial bending moment m_r is a maximum at the centre where $\partial^2 m_r/\partial\rho^2|_{\rho=0}\leqslant 0$.

3.5. *Motion beginning in mechanism 3b*

For the motion beginning in mechanism 2a, if the peak pressure μ_0 is greater than μ_{23ab} for $0.457<\alpha<0.63$, the condition that the radial bending moment m_r is a maximum at the centre is violated; for the motion beginning in mechanism 2b if the peak pressure μ_0 is greater than μ_{23b} for $0.63<\alpha\leqslant 1$, the condition $m_r\geqslant 0$ in the neighbourhood of $\rho=1$ is not satisfied. This suggests that the velocity field of mechanism 3b consists of a central portion $0\leqslant\rho\leqslant\rho_0$ moving with a uniform velocity $\dot{w}_0$, an annulus $\rho_0\leqslant\rho\leqslant\rho_1$ having a linear velocity distribution with respect to ρ and an annulus $\rho_1\leqslant\rho\leqslant 1$ having a logarithmic velocity distribution with respect to ρ [Fig. 1(e)]. Thus the velocity pattern of mechanism 3b is

$$\dot{w}(\rho,t)=\begin{cases}\dot{w}_0(t) & 0\leqslant\rho\leqslant\rho_0(t)\\ \dot{w}_0(t)[1-\sigma_2(\rho-\rho_0)/\rho_1] & \rho_0(t)\leqslant\rho\leqslant\rho_1(t)\\ \dot{w}_0(t)\sigma_2\ln\dfrac{1}{\rho} & \rho_1(t)\leqslant\rho\leqslant 1\end{cases}\tag{25}$$

where $\sigma_2=[\ln(1/\rho_1)+1-(\rho_0/\rho_1)]^{-1}$. Corresponding to the above velocity pattern, the flow rules require that m_r and m_θ in portion $0\leqslant\rho\leqslant\rho_0$ are in regime A, while moments in portion $\rho_0\leqslant\rho\leqslant\rho_1$ are in regime AB and moments in portion $\rho_1\leqslant\rho\leqslant 1$ are in regime BC.

Substituting the velocity field and the bending moment state for mechanism 3b into the equations of motion produces

$$2v^2\ddot{w}_0=\mu_0 f(t)\tag{26}$$

$$v^2\ddot{w}_0\eta\{2\xi_1(3-3\eta+\eta^2)+\eta(6-8\eta+3\eta^2)\}(\xi_1+\eta)-v^2\dot{w}_0\dot{\xi}_1\eta^2\{\eta(1-\eta)(4-3\eta)$$
$$+\xi_1(6-8\eta+3\eta^2)\}-v^2\dot{w}_0\dot{\eta}\eta^2\{\eta(4-3\eta)+2\xi_1(3-2\eta)\}$$
$$=\begin{cases}\{\mu_0 f(t)[3\alpha^2 e^{2\xi_1}-(1-\eta)^3-2\alpha^3 e^{3\xi_1}]-3e^{2\xi_1}\}(\xi_1+\eta)^2 & (\rho_1>\alpha)\\ \{\mu_0 f(t)\eta(3-3\eta+\eta^2)-3e^{2\xi_1}\}(\xi_1+\eta)^2 & (\rho_1\leqslant\alpha)\end{cases} \tag{27}$$

$$v^2\ddot{w}_0\{3e^{2\xi_1}-3-2\xi_1(3-3\eta+3\eta^2-\eta^3)\}(\xi_1+\eta)+v^2\dot{w}_0\dot{\xi}_1$$
$$\times\{-3e^{2\xi_1}+3+2\xi_1[3-\eta^2(1-\eta)(3-2\eta)]-2\xi_1^2(2\eta^3-6\eta^2+6\eta-3)\}$$
$$+v^2\dot{w}_0\dot{\eta}\{-3e^{2\xi_1}+3+2\xi_1[3-\eta^2(3-2\eta)]+6\xi_1^2(1-\eta)^2\}$$
$$=\begin{cases}3(\mu_0 f(t)\alpha^2-1)\xi_1(\xi_1+\eta)^2 e^{2\xi_1} & (\rho_1>\alpha)\\ 3\left\{\frac{1}{2}\mu_0 f(t)\alpha^2\left(1+2\ln\frac{1}{\alpha}-\frac{e^{2\xi_1}}{\alpha^2}\right)-\xi_1\right\}(\xi_1+\eta)^2 e^{2\xi_1} & (\rho_1\leqslant\alpha)\end{cases} \tag{28}$$

where $\xi_1=\ln(1/\rho_1)$ and $\eta=1-(\rho_0/\rho_1)$.

Now for larger loaded radius and somewhat larger pressures

$$\mu_{23ab}<\mu_0\leqslant\mu_{34b}\quad 0.457<\alpha\leqslant 0.63$$
$$\mu_{23b}<\mu_0\leqslant\mu_{34b}\quad 0.63\ <\alpha\leqslant 1 \tag{29}$$

the plate begins to deform in mechanism 3b (Fig. 4) if the minimum value of the radial bending moment $m_r(\rho_2)$ in portion $\rho_1\leqslant\rho\leqslant 1$ does not exceed the negative fully plastic bending moment.

3.6. *Motion beginning in mechanism* 4

If $\mu_0>\mu_{34a}$ when $0<\alpha<0.457$ and $\mu_0>\mu_{34b}$ when $0.457<\alpha\leqslant 1$, it is assumed that the initial velocity pattern consists of a central portion of radius ρ_0 moving at a velocity $\dot{w}_0$, and a middle annular portion $\rho_0\leqslant\rho\leqslant\rho_1$ having a linear velocity distribution with respect to ρ and an outer annular portion $\rho_1\leqslant\rho\leqslant 1$ where the velocity varies logarithmically with ρ [Fig. 1(f)]. This velocity pattern produces a discontinuity of the radial rate of rotation across the circle of radius ρ_2. At $\rho=\rho_0$ and $\rho=\rho_2$, two plastic hinge circles exist [Fig. 1(f)]. Compatible with the above assumption on the plate deformation mechanism, bending moments in the portion $0\leqslant\rho\leqslant\rho_0$ are at vertex A (regime A) of the Tresca yield condition, in the portion $\rho_0\leqslant\rho\leqslant\rho_2$ are on sides AB (regime AB) and BC (regime BC), and in the portion $\rho_2\leqslant\rho\leqslant 1$ are on side CB (regime BC).

Employing the normality rule and using continuities of radial angular rate of rotation across the circle ρ_0 and of transverse velocity across the circle ρ_2, integration gives the velocity field,

$$\dot{w}=\begin{cases}\dot{w}_0 & 0\leqslant\rho\leqslant\rho_0(t)\\ \dot{w}_2+(\dot{w}_0-\dot{w}_2)[1-\sigma_3(\rho-\rho_0)/\rho_1] & \rho_0(t)\leqslant\rho\leqslant\rho_1(t)\\ \dot{w}_2+(\dot{w}_0-\dot{w}_2)\sigma_3\ln\dfrac{\rho_2}{\rho} & \rho_1(t)\leqslant\rho\leqslant\rho_2(t)\\ \dot{w}_2\dfrac{\ln\rho}{\ln\rho_2} & \rho_2(t)\leqslant\rho\leqslant 1\end{cases} \tag{30}$$

where $\sigma_3=[\ln(\rho_2/\rho_1)+1-(\rho_0/\rho_1)]^{-1}$ and $\dot{w}_2$ is the transverse velocity at radius $\rho=\rho_2$.

Substituting the above velocity pattern and bending moment yield conditions into the equations of motion and using transformations $\xi_1=\ln(1/\rho_1)$, $\xi_2=\ln(1/\rho_2)$, $\eta=1-\rho_0/\rho_1$

gives the following equations

$$2v^2\ddot{w}_0 = \mu_0 f(t) \tag{31}$$

$$\begin{aligned}
&v^2\ddot{w}_2\eta^3(2-\eta)(\xi_1-\xi_2+\eta)+v^2\ddot{w}_0\eta\{2(\xi_1-\xi_2)(3-3\eta+\eta^2)\\
&\quad+\eta(6-8\eta+3\eta^2)\}(\xi_1-\xi_2+\eta)-v^2(\dot{w}_0-\dot{w}_2)\dot{\xi}_1\eta^2\{\eta(1-\eta)(4-3\eta)\\
&\quad+(\xi_1-\xi_2)(6-8\eta+3\eta^2)\}-v^2(\dot{w}_0-\dot{w}_2)\dot{\xi}_2\eta^3(2-\eta)\\
&\quad-v^2(\dot{w}_0-\dot{w}_2)\dot{\eta}\eta^2\{\eta(4-3\eta)+2(\xi_1-\xi_2)(3-2\eta)\}\\
&=\begin{cases}\{\mu_0 f(t)[3\alpha^2\,\mathrm{e}^{2\xi_1}-(1-\eta)^3-2\alpha^3\,\mathrm{e}^{3\xi_1}]-3\mathrm{e}^{2\xi_1}\}(\xi_1-\xi_2+\eta)^2 & (\rho_1>\alpha)\\ \{\mu_0 f(t)\eta(3-3\eta+\eta^2)-3\,\mathrm{e}^{2\xi_1}\}(\xi_1-\xi_2+\eta)^2 & (\rho_1\leqslant\alpha)\end{cases}
\end{aligned} \tag{32}$$

$$\begin{aligned}
&v^2\ddot{w}_2\{3(\xi_1-\xi_2+\eta-1)\,\mathrm{e}^{2(\xi_1-\xi_2)}+(\xi_1-\xi_2)(3-6\eta+6\eta^2-2\eta^3)\\
&\quad+3(1-\eta)\}(\xi_1-\xi_2+\eta)+v^2\ddot{w}_0\{3\,\mathrm{e}^{2(\xi_1-\xi_2)}-3-2(\xi_1-\xi_2)(3-3\eta+3\eta^2-\eta^3)\}\\
&\quad\times(\xi_1-\xi_2+\eta)+v^2(\dot{w}_0-\dot{w}_2)\dot{\xi}_1\{-3\,\mathrm{e}^{2(\xi_1-\xi_2)}+3+2(\xi_1-\xi_2)[3-\eta^2(1-\eta)(3-2\eta)]\\
&\quad-2(\xi_1-\xi_2)^2(2\eta^3-6\eta^2+6\eta-3)\}+v^2(\dot{w}_0-\dot{w}_2)\dot{\xi}_2\{3[1-\eta-(\xi_1-\xi_2)]\,\mathrm{e}^{2(\xi_1-\xi_2)}\\
&\quad+(\xi_1-\xi_2)(2\eta^3-6\eta^2+6\eta-3)+3(\eta-1)\}+v^2(\dot{w}_0-\dot{w}_2)\dot{\eta}\\
&\quad\times\{-3\,\mathrm{e}^{2(\xi_1-\xi_2)}+3+2(\xi_1-\xi_2)[3-\eta^2(3-2\eta)]+6(\xi_1-\xi_2)^2(1-\eta)^2\}\\
&=\begin{cases}3\{[\mu_0 f(t)\alpha^2-1](\xi_1-\xi_2)-1\}(\xi_1-\xi_2+\eta)^2\,\mathrm{e}^{2\xi_1} & (\rho_1>\alpha)\\ 3\left\{\dfrac{1}{2}\mu_0 f(t)\alpha^2\left(1-2\xi_2+2\ln\dfrac{1}{\alpha}-\dfrac{\mathrm{e}^{-2\xi_1}}{\alpha^2}\right)\right.\\ \qquad\left.-(1+\xi_1-\xi_2)\right\}(\xi_1-\xi_2+\eta)^2\mathrm{e}^{2\xi_1} & (\rho_1\leqslant\alpha)\end{cases}
\end{aligned} \tag{33}$$

$$\begin{aligned}
&v^2\ddot{w}_2\{3\,\mathrm{e}^{2(\xi_1-\xi_2)}[2(\xi_1-\xi_2)+2\eta-1]+3-2\eta(3-3\eta+\eta^2)\}(\xi_1-\xi_2+\eta)\\
&\quad+v^2\ddot{w}_0\{3\,\mathrm{e}^{2(\xi_1-\xi_2)}-3+2\eta(3-3\eta+\eta^2)\}(\xi_1-\xi_2+\eta)+v^2(\dot{w}_0-\dot{w}_2)\dot{\xi}_1\\
&\quad\times\{-3\,\mathrm{e}^{2(\xi_1-\xi_2)}-2(\xi_1-\xi_2)(2\eta^3-6\eta^2+6\eta-3)+3-2\eta^2(1-\eta)(3-2\eta)\}\\
&\quad+v^2(\dot{w}_0-\dot{w}_2)\dot{\xi}_2\{3[1-2\eta-2(\xi_1-\xi_2)]\,\mathrm{e}^{2(\xi_1-\xi_2)}+2\eta^3-6\eta^2+6\eta-3\}\\
&\quad+v^2(\dot{w}_0-\dot{w}_2)\dot{\eta}\{-3\,\mathrm{e}^{2(\xi_1-\xi_2)}+3-2\eta^2(3-2\eta)+6(\xi_1-\xi_2)(1-\eta)^2\}\\
&=3(\mu_0 f(t)\alpha^2-1)(\xi_1-\xi_2+\eta)^2\,\mathrm{e}^{2\xi_1}
\end{aligned} \tag{34}$$

$$-v^2\ddot{w}_2\xi_2(-\mathrm{e}^{2\xi_2}+1+2\xi_2+2\xi_2^2)+v^2\dot{w}_2\dot{\xi}_2(-\mathrm{e}^{2\xi_2}+1+2\xi_2+2\xi_2^2)=\xi_2^2\mathrm{e}^{2\xi_2}. \tag{35}$$

In the above, mechanisms 2b and 1 have been discussed previously by Conroy (1969), Hopkins and Prager (1954) and Youngdahl (1971, 1987). The velocity patterns of these two mechanisms are linear with respect to ρ and the corresponding radial bending moment is greater than or equal to zero everywhere. These two mechanisms are just suitable for low pressure μ_0 (the area below the broken line in Fig. 4). Above the broken line four new deformation mechanisms are found in which velocity fields include an annular portion with a logarithmic velocity distribution—the radial bending moment is negative in this portion.

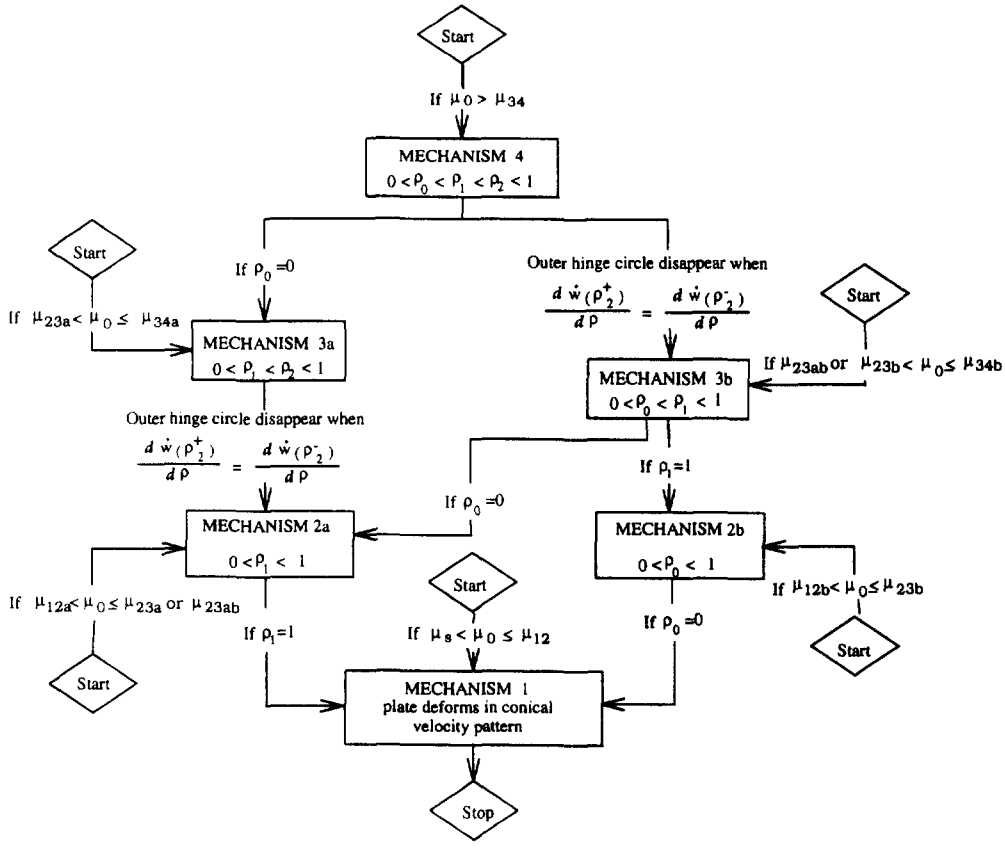

Fig. 5. Ensuing mechanisms after the plate motion begins in one of six mechanisms. For decreasing pressure the deformation mechanism evolves after initiation in one of six mechanisms. The independent mechanisms are identified in terms of different hinge circles. After unloading these circles move towards either the center or the periphery where they disappear.

3.7. *Deformation process for decreasing pressures*

For the motion beginning in mechanism 1 the plate deformation ceases when $\dot{w}_0 = 0$; for the other initial mechanisms, the deformation begins in a transient phase involving travelling hinge circles at $\rho = \rho_0(t)$, $\rho = \rho_2(t)$ and the travelling circle of radius $\rho_1(t)$, followed by a modal phase of deformation in mechanism 1. In this process of motion, deformation may change its velocity pattern when one of the circles at $\rho = \rho_0$, ρ_1 or ρ_2 reaches its terminal position (Fig. 5).

4. SOLUTION FOR RECTANGULAR PULSE

As discussed in the section on mechanism 2a, the equations for the initial hinge radius $\rho_1(0)$ are (13) and (14). The initial positions of the hinges ρ_0, ρ_1 and ρ_2 are calculated numerically with the use of an iteration subroutine for non-linear algebraic equations from the NAG Fortran library. After the initial positions of ρ_0, ρ_1 and ρ_2 have been obtained, a subroutine from the NAG Fortran library efficiently integrates the governing equations to obtain the motion initiated by a rectangular pressure pulse and finally the central deflection Δ. These systems of non-linear equations seem well-behaved; there has been no evidence of singularities or lack of uniqueness. The following discussion focuses on deformation mechanisms in a plate if the motion begins in deformation mechanism 4. For the other initial mechanisms the details are simpler.

For a constant pressure p_0, the calculation shows that the initial values of ξ_1, ξ_2, η given by the initial condition $\dot{w}(\rho, 0) = 0$ do not vary with time during the loading period t_0. This means the hinge circles and the circle of radius ρ_1 remain stationary while the pressure is constant. Before the constant pressure is removed at time $t = t_0$, the motion

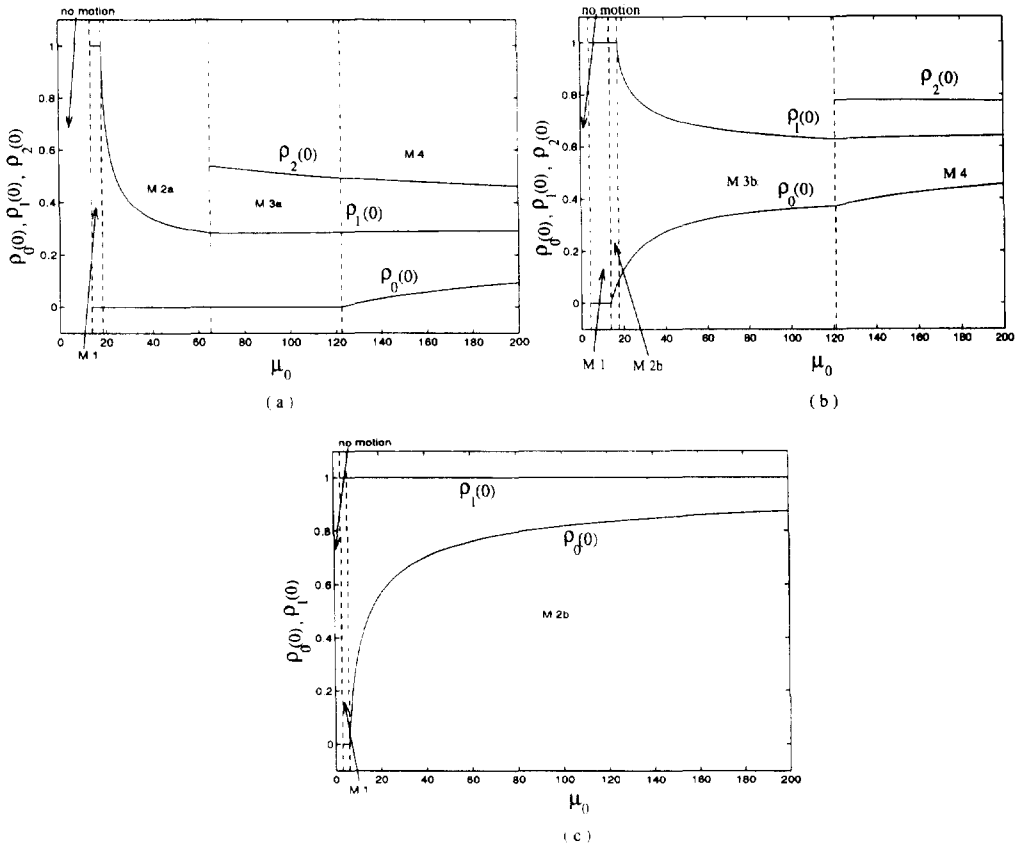

Fig. 6. Initial values of radii ρ_0, ρ_1, ρ_2 as a function of pressure intensity.

involves the equations for the initial values of ξ_1, ξ_2, η given in the previous section. The corresponding solution of initial values for radii ρ_0, ρ_1 and ρ_2, which are denoted by $\rho_0(0)$, $\rho_1(0)$ and $\rho_2(0)$, are shown in Fig. 6 as functions of the load magnitude μ_0 for $\alpha = 0.3$, 0.65 and 1, respectively. It can be seen that for $\alpha = 1$ [Fig. 6(c)], the circle of radius $\rho_1(0)$ is at the plate support and the outer hinge circle does not appear at all; $\rho_0(0)$ becomes much larger for more intense pressure if $\mu_0 \leqslant 90$; for even larger pressures the periphery of the central flat region $\rho_0(0)$ gradually approaches unity which is the initial value for an impulsively loaded plate. For $\alpha = 0.3$ and 0.65 [Figs 6(a, b)], if the outer hinge circle does not appear, $\rho_0(0)$ and $\rho_1(0)$ vary rapidly with increasing pressure μ_0 until $\rho_1(0)$ is equal to α [intersection of dotted line and $\rho_1(0)$]. Later the radii of hinge circles change slowly; if the outer hinge circle does appear in a plate under very intense pressure, the radii of all hinge circles $\rho_0(0)$, $\rho_1(0)$, $\rho_2(0)$ change slowly and tend to the radius of loading, α, as μ_0 increases.

For a constant pressure μ_0, a plate deforming in mechanism 4 will have a radial bending moment m_r that is uniform in the central portion $0 \leqslant \rho \leqslant \rho_0$,

$$m_r = 1. \tag{36}$$

In the annulus $\rho_0 \leqslant \rho < \rho_1$,

$$\begin{aligned} m_r = {} & 1 + (\dot{w}_0 - \dot{w}_2)[2(1 + \xi_1 - \xi_2)(\rho^3 - 3\rho\rho_0^2 + 2\rho_0^3) - e^{\xi_1}(\rho^4 - 4\rho\rho_0^3 \\ & + 3\rho_0^4)]\, e^{2\xi_1}/3\rho + 2\dot{w}_2(\rho^3 - 3\rho\rho_0^2 + 2\rho_0^3)\, e^{2\xi_1}(\xi_1 - \xi_2 + \eta)/3\rho \\ & - \begin{cases} \mu_0(\rho^3 - 3\rho\rho_0^2 + 2\rho_0^3)/3\rho & (\alpha > \rho) \\ \mu_0[(\alpha^3 - 3\alpha\rho_0^2 + 2\rho_0^3)/3\rho + (\alpha^2 - \rho_0^2)(\rho - \alpha)/\rho] & (\alpha \leqslant \rho) \end{cases} \end{aligned} \tag{37}$$

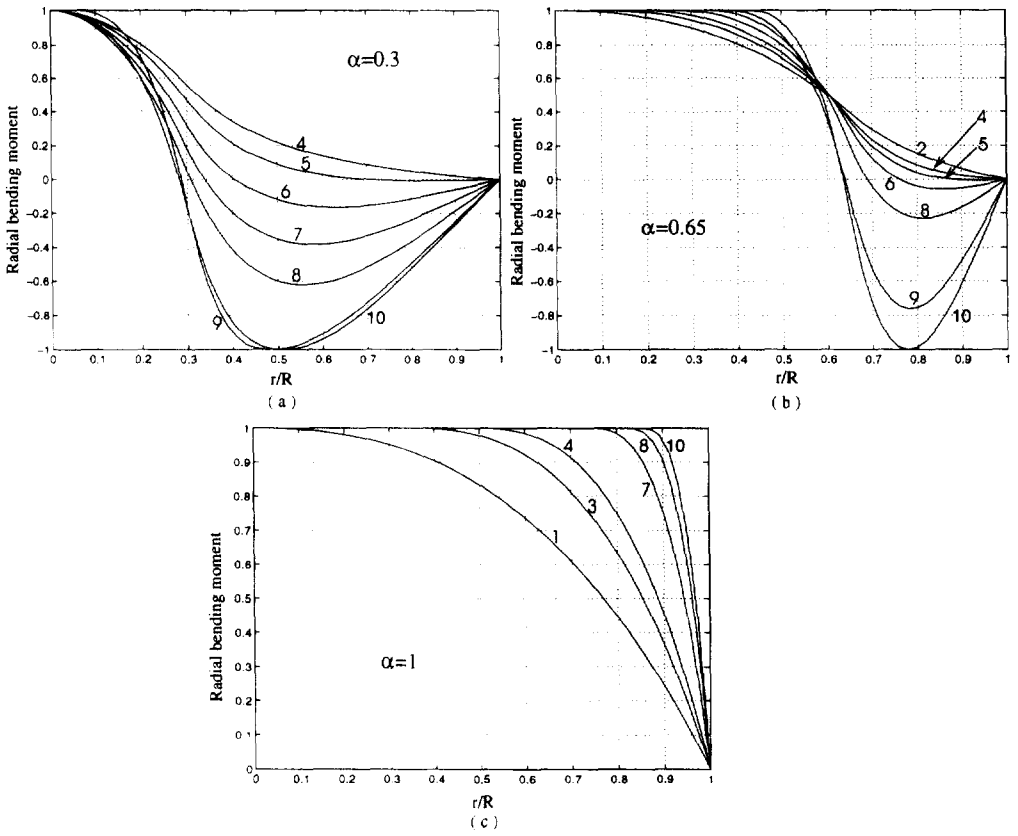

Fig. 7. Distribution of radial bending moment in plate for increasing pressure (a) $\alpha = 0.3$; (b) $\alpha = 0.65$; (c) $\alpha = 1$. Curve number 1 for $\mu_0 = 5$, 2 for $\mu_0 = 8$, 3 for $\mu_0 = 10$, 4 for $\mu_0 = 15$, 5 for $\mu_0 = 20$, 6 for $\mu_0 = 30$, 7 for $\mu_0 = 40$, 8 for $\mu_0 = 50$, 9 for $\mu_0 = 100$ and 10 for $\mu_0 = 150$.

In the annulus $\rho_1 \leqslant \rho < \rho_2$,

$$\begin{aligned} m_r &= \ln(\rho/\rho_1) + 2(\dot{w}_0 - \dot{w}_2)[3(\xi_1 - \xi_2) + \eta(3 - 3\eta + \eta^2)]\ln(\rho/\rho_1)/3 \\ &\quad - e^{2\xi_1}(\dot{w}_0 - \dot{w}_2)[\rho^2 \ln\rho - \rho^2 + \rho_1^2(1+\xi_1) + \rho_1^2(1+2\xi_1)\ln(\rho/\rho_1)] \\ &\quad + \dot{w}_2 e^{2\xi_1}(\rho^2 - \rho_1^2)(\xi_1 - \xi_2 + \eta) \\ &\quad - \begin{cases} \mu_0[(\alpha^2 - \rho_1^2)/2 - \alpha^2 \ln(\rho/\alpha)] & (\rho > \alpha, \rho_1 < \alpha) \\ \mu_0 \alpha^2 \ln(\rho/\rho_1) & (\rho > \alpha, \rho_1 \geqslant \alpha) \\ \mu_0(\alpha^2 - \rho_1^2)/2 & (\rho \leqslant \alpha) \end{cases} \end{aligned} \tag{38}$$

In the outer portion $\rho_2 \leqslant \rho \leqslant 1$,

$$m_r = -1 - \dot{w}_2[\rho^2 \ln\rho - \rho^2 + \rho_2^2(1+\xi_2) + \rho_2^2(1+2\xi_2)\ln(\rho/\rho_2)]\, e^{2\xi_1}(\xi_1 - \xi_2 + \eta)/\xi_2. \tag{39}$$

For other mechanisms, some of the hinges may not exist and correspondingly some regions bounded by the hinges may not appear. For other mechanisms the radial bending moment distributions are expressed by the above equations as well after portions are excluded which do not exist for the corresponding mechanism. From Fig. 7 it is clear that the radial bending moment under different pressures does not violate the yield condition.

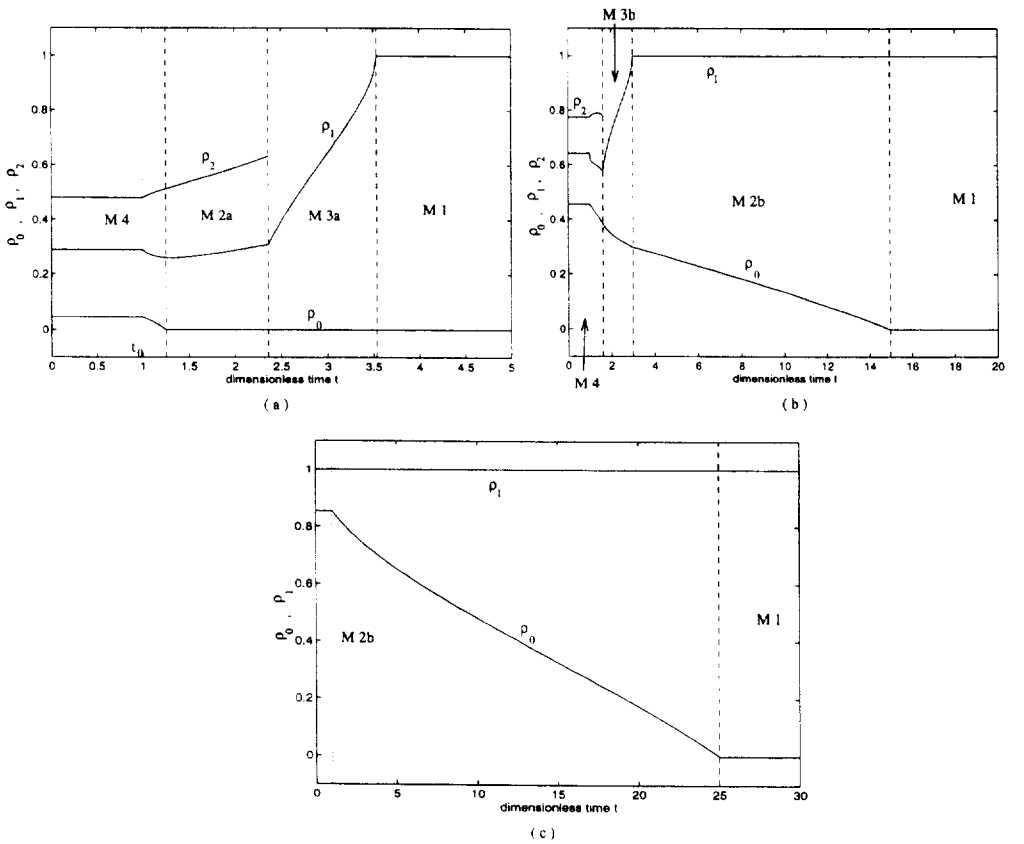

Fig. 8. Variation of hinge radii ρ_0, ρ_1 and ρ_2 with t for (a) $\alpha = 0.3$ and $\mu_0 = 150$; (b) $\alpha = 0.65$ and $\mu_0 = 200$; (c) $\alpha = 1$ and $\mu_0 = 150$.

After the constant pressure is removed at time $t = t_0$, the hinge radii ρ_0, ρ_1 and ρ_2 begin to vary (see Fig. 8). It can be seen that for a small radius of loading, $\alpha = 0.3$, the inner hinge circle at $\rho = \rho_0$ reaches its terminal position first while for a large radius of loading, $\alpha = 0.65$, the outer hinge circle at $\rho = \rho_2$ disappears first [Figs 8(a,b)]. In Fig. 8, the different deformation mechanisms are bounded by broken lines. It is clear that for a small radius of loading, $\alpha = 0.3$, the outer hinge circle at $\rho = \rho_2$ exists much longer than it does for a large radius of loading, $\alpha = 0.65$, because for the large radius of loading the outer hinge circle is closer to the boundary. In both cases the circle of radius $\rho = \rho_1$ increases in radius dramatically after the outer hinge circle at $\rho = \rho_2$ disappears. The reason may be that after the outer hinge circle disappears the boundary condition begins to influence the motion of the circle of radius $\rho = \rho_1$ significantly since the negative fully plastic bending moment at the outer hinge circle acts like a clamped plate. Our calculation for the above values of α shows that after pressure is removed, the ensuing hinge patterns follow a unique path along the direction normal to the α axis; however, a proof has not been obtained for the general case.

A solution for bending deformation of a clamped plate by a central pressure pulse was given by Florence (1966a,b). In Florence's solution the bending moments m_r and m_θ at the centre of a clamped plate are in regime A of the Tresca yield condition while the moments at the periphery are in regime C. Corresponding to regime C, the outer hinge of radius ρ_2 exists in any deformation mechanism while the circle of radius ρ_1 is always located between the plate centre and the periphery of the plate. The annulus between the outer hinge circle and the periphery $\rho_2 \leqslant \rho \leqslant 1$ is stationary.

For a plate subjected to a constant pressure μ_0 for a period of time t_0, the final central deflection $\Delta = W_0 = Hw_0 = H\int_0^{t_f} \dot{w}_0 \, dt$ where t_f is the time when the plate ceases its motion. This deflection can be related to the impulse applied per unit area $I = p_0 T_0$ and the pressure magnitude μ_0 by the expression $\delta = \Delta\mu_0 M_0 / I^2 R^2 = g(\mu_0)$ for a certain radius of loading α

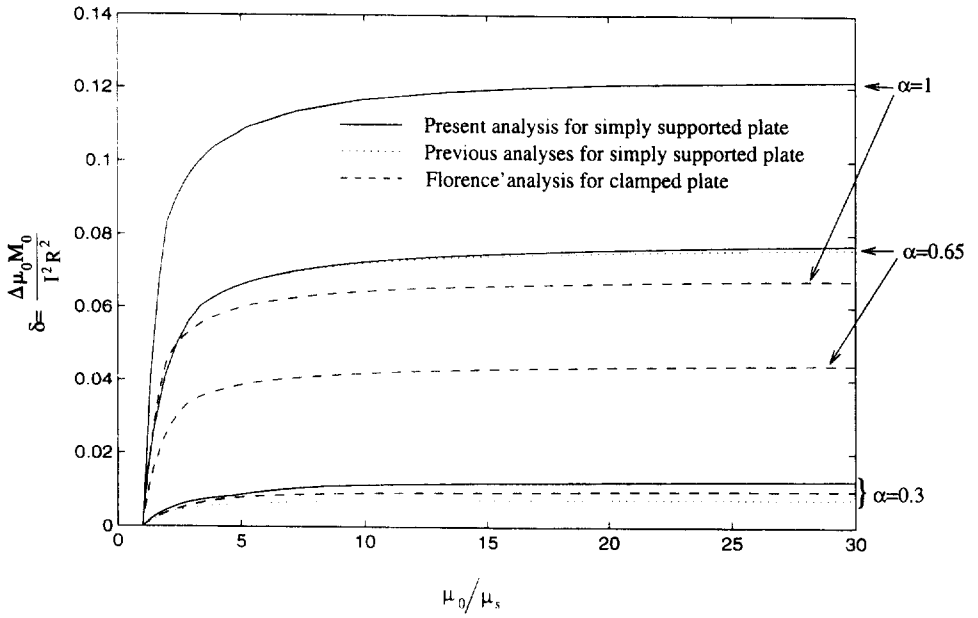

Fig. 9. Final central deflection of simply supported and clamped plates as function of pressure μ_0.

(Florence, 1966a). In Fig. 9, the non-dimensional final central deflection of a simply supported plate is calculated by the present analysis and the previous analyses which used a linear velocity field. The deflection of a clamped plate is calculated according to Florence's analysis (Florence, 1966a) for $\alpha = 0.3$, 0.65 and 1, respectively. The results of these three analyses are similar to each other in two aspects: the three curves are qualitatively similar—they start from the value $\mu_0/\mu_s = 1$ where $\delta = 0$ and tend monotonically towards horizontal asymptotes; for the same value of μ_0/μ_s, δ is larger for a larger radius of loading. Nevertheless it is found that the central deflection δ of simply supported plates is larger than that of clamped plates. It can be seen that the difference between the values of δ for simply supported plates and clamped plates increases with α; this means that for simply supported plates the boundary conditions have more influence for larger loading radius α. It is also clear that for a simply supported plate if the radius of loading is small, $\alpha = 0.3$, the initial velocity field of previous analyses which do not give moments that satisfy yield results in a central deflection δ which is much smaller than that predicted by the present complete analysis, i.e. the kinematically admissible velocity field has over-constrained the deformations (Stronge and Yu, 1993, p. 40). For a large radius of loading the central deflection is insensitive to the initial velocity field.

5. CONCLUSIONS

From the above discussion, the following conclusions can be drawn.

(1) For high pressures, the deformation mechanisms used by previous authors do not satisfy the yield criterion. Four additional mechanisms which satisfy yield have been described.

(2) For any pressure on equal size plates, a simply supported plate has larger deflection than an identical plate which is clamped at the edge. The difference between centre deflection of simply supported and clamped plates becomes largest as the loading region becomes more extensive.

(3) For a small radius of loading (e.g. $\alpha = 0.3$), the central deflection resulting from the non-linear velocity distribution of the present analysis is much larger than that predicted by the linear velocity pattern assumed in the previous analyses. For a large radius of loading ($\alpha \geqslant 0.65$), the error introduced by assuming a linear velocity field does not change the calculated final deflections very much. For a very large applied pressure, the previous

analyses did not satisfy the yield condition: only the present analysis results in bending moments that satisfy yield throughout the plate.

Acknowledgements—Dongquan Liu would like to thank British Gas for financial support and Trinity College for a Research Scholarship.

REFERENCES

Conroy, M. F. (1969). Rigid–plastic analysis of a simply supported circular plate due to dynamic circular loading. *J. Franklin Inst.* **288,** 121–135.

Florence, A. L. (1966a). Clamped circular plates under central blast loading. *Int. J. Solids Structures* **2,** 319–335.

Florence, A. L. (1966b). Clamped circular rigid–plastic plates under blast loading. *J. Appl. Mech.* **33,** 256–260.

Hopkins, H. G. and Prager, W. (1953). The load carrying capacities of circular plates. *J. Mech. Phys. Solids* **2,** 1–13.

Hopkins, H. G. and Prager, W. (1954). On the dynamics of plastic circular plates. *J. Appl. Math. Phys. ZAMP* **5,** 317–330.

Jones, N. and Song, B. (1986). Shear and bending response of a rigid–plastic beam to partly distributed blast-type loading. *J. Struct. Mech.* **14,** 275–320.

Stronge, W. J. and Yu, T. X. (1993). *Dynamic Models for Structural Plasticity*. Springer, London.

Youngdahl, C. K. (1971). Influence of pulse shape on the final plastic deformation of a circular plate. *Int. J. Solids Structures* **7,** 1127–1142.

Youngdahl, C. K. (1987). Effect of pulse shape and distribution on the plastic deformation of a circular plate. *Int. J. Solids Structures* **23,** 1179–1189.